ACS OMEGA

http://pubs.acs.org/journal/acsodf

Article

Modification of Metal (Fe, Al) Doping on Reaction Properties of a NiO Oxygen Carrier with CO during Chemical Looping Combustion

Shubo Chen, Wenguo Xiang,* and Shiyi Chen*

Cite This: *ACS Omega* 2022, 7, 4381−4388

Read Online

ACCESS | Metrics & More | Article Recommendations

ABSTRACT: Oxygen carriers can significantly enhance the performance of chemical looping combustion at low energy-cost CO_2 capture. Based on the density functional theory, a microscopic model of the metal Fe, Al-doped NiO oxygen carrier was established. The results indicate that the intermediate state energy and the reaction energy reduce due to electronic interaction of the Al-doped surface. With the progress of the reaction, the NiO−Al surface promotes the oxidation process of CO, indicating that the activity of the NiO surface enhanced, which is attributed to the electronic and steric effects of the Al−O structure. For the decomposition of CO on the OC surface, doping with other atoms is beneficial to suppress the carbon deposition, which is related to the steric hindrance caused by doping with other atoms. Besides, doping with iron and aluminum atoms is more conducive to the movement of OC bulk crystal lattice oxygen to the surface, thereby promoting subsequent reactions. Therefore, it is feasible to improve the reactivity of the Ni-based OC by doping metal Al, and its modification effect is closely related to the characteristics of the components.

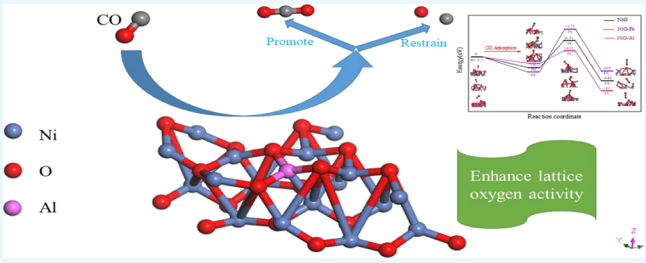

1. INTRODUCTION

Chemical looping combustion (CLC) is an innovative energy conversion technology that achieves low-cost CO_2 capture. It utilizes the oxygen carrier (OC), which shifts the oxygen in the air to the fuel in the form of lattice oxygen, continuously circulating between the air reactor and the fuel reactor, as shown in Figure 1.[1] The advantage of this technology is the internal separation of CO_2 in the flue gas, which greatly reduces the cost of carbon separation.[2,3] In addition, CLC also has the advantages of low NO_x generation and good gas selectivity.[4,5]

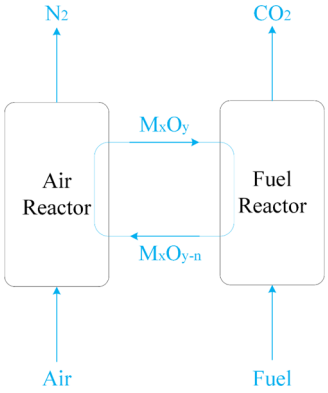

Figure 1. CLC schematic diagram.

In CLC, the OC is one of the key factors in the CLC system. OC reactivities that promotes redox reactions and bulk oxygen mobility are essential consideration, as they will significantly affect the design of the reactor and the operation of the process.[6−9] It is necessary to consider OC reaction activity such as promotion of redox reaction, generation of oxygen ions, and body oxygen mobility.[10,11] As the common OC, metal oxides, mainly including transition metals such as Ni, Cu, Fe, Co, Mn, and so forth, have the advantages of fast reaction speed, high mechanical stability and recyclability, and high temperature resistance.[12−15] Because NiO has good kinetic properties and favorable catalytic ability to break carbon−hydrogen bonds, the Ni-based OC can almost achieve 100% conversion of hydrocarbon fuels.[16,17] NiO exhibits high reactivity and high upper operating temperature limit. NiO is currently one of the most promising OC materials.[18] However, there are some challenges in the application of NiO OC. Mainly, some reactions (reaction 1 and reaction 2) cause deactivation due to carbon deposition beyond the OC surface.[19]

Received: November 3, 2021
Accepted: January 20, 2022
Published: January 29, 2022

ACS Publications

© 2022 The Authors. Published by American Chemical Society

$$CH_4 \rightarrow C + 2H_2 \quad (1)$$

$$2CO \rightarrow C + CO_2 \quad (2)$$

To avoid sintering, inert carriers such as Al_2O_3, $NiAl_2O_4$, and other spinel structures are commonly added to enhance the stability of OC.[20−22] Lucia et al. pointed out the $NiAl_2O_4$ additive contribution to oxidize the fuel in CLC.[20] Zhang et al. also reported that $NiO/NiAl_2O_4$ exhibits high stability and good activity.[22] Moheddin et al. reported that NiO/Al_2O_3−ZrO_2−CeO_2 is considered as a potential effective OC in CLC.[23] Therefore, the Ni-based OC supported by the inert carrier, especially Al_2O_3, has a very high reactivity, which can achieve almost 100% conversion of hydrocarbon fuels and have a higher CLC efficiency.

In addition, due to the synergistic effect, the doping of metal oxides to form a composite metal oxide can also further enhance the performance of OC. The combination of different metals could form some distinctive (or special) structures, such as spinel and perovskites.[24,25] Deng et al. showed that the specific surface of the modified metal oxide has been enhanced, with enhanced heat transfer performance.[26] Hossain et al. showed that the activation energy of the reaction between H_2 and the Co-doped Ni/Al_2O_3 OC decreases.[27] Doping with other metals can provide active sites to decrease surface energy barrier, thereby improving surface reaction performance.[28,29] Kuo et al. reported that Fe-modified nickel-based OC showed better reactivity and recycling characteristics in the chemical looping process.[30] Ma et al. reported that $NiFe_2O_4$ doped with CeO_2 performed best in terms of cyclability and phase stability during the redox cycle.[31] Thus, the doping component has a great influence on the structure of the Ni-based OC and its reactivity.

Although there have been a large number of experiments on the modification of OCs to enhance the performance of composite OCs, the underlying mechanism of the OC performance enhancement is not clear yet. Currently, the experimental result is not able to provide a complete explanation on the mechanism of the OC reaction process. Theoretical research, especially the research based on density functional theory (DFT), is a complementary tool for the experimental test and can provide more detailed information. DFT has been widely used in chemical looping research. Qin et al. pointed out the reaction mechanism of NH_3 and ethanol molecules on the Fe-based OC surface.[32,33] Liang et al. verified the adsorption and reaction characteristics of the Co-doped iron oxide (104) surface.[34] Yuan et al. clarified the reaction mechanism of syngas combustion by NiO.[35] Yuan et al. also used DFT to analyze the adsorption principle of syngas and lattice oxygen transfer mechanism on the surface of pure NiO (100) behavior.[36,37]

At present, there have been some reports on the mechanism of oxygen vacancies on the surface of NiO. However, the research on the modified nickel-based OC is mainly based on experimental characterization, and there are very few studies on the microscopic doping and reaction mechanism in the molecular level. In view of the synergistic effect of Fe_2O_3−NiO and the supporting effect of Al_2O_3−NiO, therefore, this work utilized DFT to investigate the effect of other metals (Fe, Al) doping on the structure of NiO and its modification mechanism in the CO reaction process and analyze the process of surface CO oxidation and carbon deposition. Compared with experimental research, theoretical simulation can be of low cost, irreplaceable, and better controllable. It can complete a lot of research works that cannot be carried out due to experimental condition limitations. So, this research aims to investigate the modification mechanism from the atomic and molecular level and provide a theoretical reference for the OC optimization. It also reduces the resource consumption and time cost needed by the experiment.

2. COMPUTATIONAL MODEL AND METHODOLOGY

All jobs are calculated by using the CASTEP code in the Materials Studio (MS). The electronic exchange related energy is depicted by the generalized gradient approximation of the Perdew−Burke−Ernzerhof functional.[38,39] A model of NiO(100) composed of six atomic layers is established and optimized, which has been proven to be the most stable surface configuration.[36] In this study, a six-layer board with (2 × 2) periodic supercell is used to simulate the NiO(100) surface for all calculations. In order to prevent the interaction between the periodic plates, a vacuum layer with a thickness of 15 Å is established. Since the coordination number of each Ni atom on the NiO(100) surface is the same, there is only one doping site, as shown in Figure 2. In the calculation process, a plane-wave expansion is applied with the smearing of 0.005 Ha with a cutoff of 400 eV and 4 × 4 × 1 Monkhorst−Pack k-point. Other calculation parameters are shown in Table 1. The transition-state (TS) search adopted the linear/secondary synchronous transition method.[40]

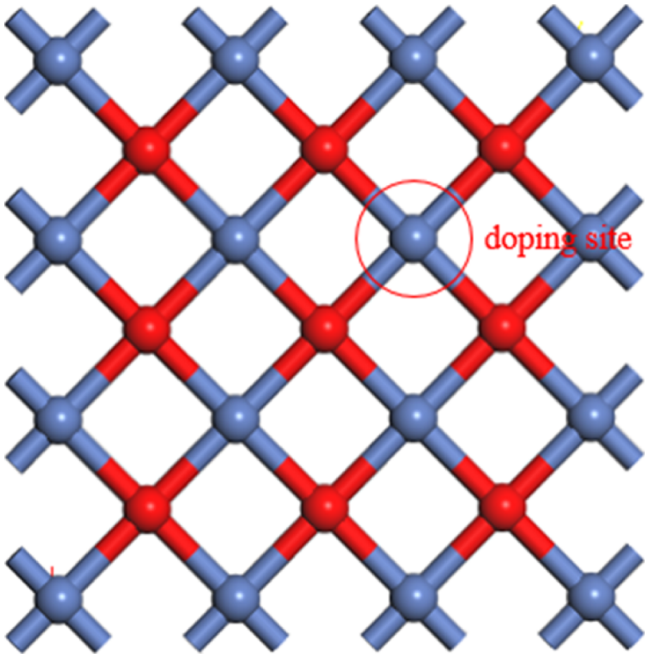

Figure 2. Doping site on the NiO (1 0 0) surface.

For each reaction, activation energy (E_b) and the reaction energy (ΔH) are defined as follows

Table 1. Calculation Parameters

parameter	value
energy tolerance	2.0×10^{-5} eV/atom
SCF tolerance	2.0×10^{-6} eV/atom
maximum force tolerance	0.5 eV/nm
maximum displacement tolerance	0.0002 nm

https://doi.org/10.1021/acsomega.1c06182
ACS Omega 2022, 7, 4381−4388

$$\Delta H = E_{FS} - E_{IS} \quad (3)$$

$$E_b = E_{TS} - E_{IS} \quad (4)$$

where E_{IS}, E_{TS}, and E_{FS} are used to describe the energies of the initial state (IS), TS, and final state (FS), respectively.

3. RESULTS AND DISCUSSION

3.1. Modification of Metal (Fe, Al)-Doping Model. The surface models of pure NiO(100) and NiO(100) modified with iron and aluminum are shown in Figure 3. In the chemical looping process, the bonding parameters, electronic density of states (DOS), and surface energy of OC determine its reaction activity. Therefore, we can compare the changes of these parameters to evaluate the ability of other atoms to modify the structure distribution of the NiO surface. In order to analyze the difficulty of doping Fe and Al atoms at the atomic sites on the NiO surface, the binding energy (E_{bind}) of Fe and Al doped was calculated

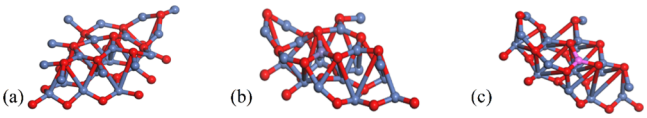

Figure 3. Stable configuration of (a) pure NiO(100), (b) Fe−NiO(100), and (c) Al−NiO(100) surfaces.

$$E_{bind} = E_{(X-NiO)} - (E_{NiO} - E_{Ni}) - E_X \quad (5)$$

In the formula, $E_{(X-NiO)}$ is the total energy of the system after X (Fe, Al) doping, $E_{(NiO)}$ is the total energy of the pure NiO system, and $E_{(Ni)}$ and $E_{(X)}$ are total energy of the atom Ni and X, respectively.

In addition, the effect of doping with other metal atoms on the bonding of O atoms on the surface is also considered. The binding energy of Fe and Al atoms doped on the NiO surface and the average bond length of O atoms adjacent to the doping site (L_{O-X}) is listed in Table 2. Both Fe and Al doping processes are exothermic processes, and doping with Al releases more heat. According to the formula, the surface of NiO doped with Al atoms is more stable. It can be seen from the table that the bond length L of doped Al atoms becomes shorter, which is consistent with the result of binding energy.

Table 2. Bond Length of O on the Pure and X-Doped Surfaces and the Binding Energy of X-Doped (X−Fe, Al)

model	E_{bind}/eV	L_{O-X}/nm
NiO		0.186
NiO−Fe	−2.00	0.183
NiO−Al	−2.94	0.177

In order to analyze the effect of doping other atoms on the NiO(100) crystal structure, X-ray simulated diffraction analysis was performed on three OCs, and X-ray diffraction patterns were obtained, as shown in Figure 4. It can be seen that the XRD spectra of OC before and after doping with iron and aluminum atoms do not change significantly, and the diffraction peaks are slightly redshifted. This is due to the shrinkage of the NiO unit cell structure caused by the doping of other atoms. It can be considered that Fe or Al atom do not change the crystal structure of NiO and only replace Ni cations in OC, so the doping modification model is applicable.

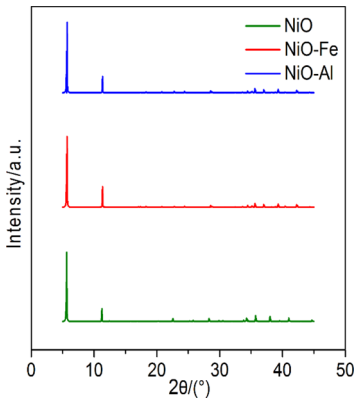

Figure 4. XRD patterns of NiO, NiO−Fe, and NiO−Al OC.

The DOSs on the surface of the system will change after Fe and Al doping. The Fe_{3d} orbital and Al_{3p} orbital are both close to the Fermi level (E_f = 0 eV) and split into bond orbitals and antibond orbitals after doping, with the doped structure stable. Figure 5 shows the DOS of Ni_{3d} curve before and after doping.

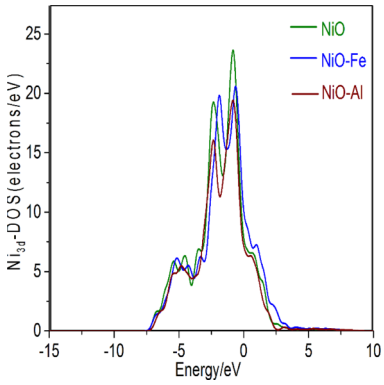

Figure 5. Ni_{3d} DOS of pure and doping surfaces.

The DOSs of the pure model and the doped model both has a strong localization in the energy range of −7 to −4 eV, and the electron delocalization is stronger in the energy range of −4 to 2 eV. In addition, the filling state energy of the pure model system close to the left side of the Fermi level is slightly higher than other doped models.

3.2. Adsorption of CO on the Surface of the Model. The adsorption of CO on the NiO surface is first investigated by approaching CO to different sites on NiO, NiO−Fe, and NiO−Al. The stable configurations of CO adsorption on these surfaces are shown in Figure 6. On the surface of pure NiO and the surface of the doped Fe atom, the CO molecule and O atom form a chemical bond, which is chemical adsorption. Bonding with the Al atom on the surface of the doped Al atom is also chemical adsorption. The bond lengths of CO

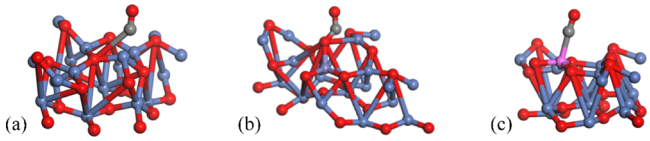

Figure 6. Stable configurations of CO absorbed on (a) pure NiO(100), (b) NiO(100)−Fe, and (c) NiO(100)−Al surfaces.

https://doi.org/10.1021/acsomega.1c06182
ACS Omega 2022, 7, 4381−4388

molecules after adsorption on the three surfaces are 0.116, 0.118, and 0.117 nm, respectively.

Adsorption energy (E_{ads}) can be used to quantitatively evaluate structural stability, and its calculation formula is as follows

$$E_{ads} = E_{CO-surface} - E_{surface} - E_{CO} \quad (6)$$

In the formula, $E_{(CO\text{-}surface)}$ is the total energy of the system after adsorption, $E_{(surface)}$ is the total energy of the OC surface, and $E_{(CO)}$ denotes the energy of the free CO molecule. Some model parameters are shown in Table 3. The CO adsorption processes on the three models are all exothermic processes, and the adsorption energies are −1.54, −1.93, and −1.18 eV, respectively. It can be seen that the heat release on the Fe-modified surface is the most, indicating that the adsorption effect is the strongest.

Table 3. Bond Length (L_{CO}) of CO and Its Charge Adsorption Energy (E_{ads}) with the Adsorbed Site after Adsorbing on Surfaces

model	E_{ads}/eV	Mulliken charge/e	C−O bond length/nm
CO		0	0.114
NiO−CO	−1.54	−0.26	0.116
NiO−Fe−CO	−1.93	0.37	0.118
NiO−Al−CO	−1.18	−0.47	0.117

Further electronic characteristic analysis is able to qualitatively detect CO adsorption on the pure and doping NiO. Charge population shows that CO becomes $CO^{0.26-}$, $CO^{0.37+}$, and $CO^{0.47-}$ after adsorption on NiO, NiO−Fe, and NiO−Al surfaces, respectively, which indicates that there is an electronic interaction between the CO molecule and the metal oxide surface. The pure surface and the doped Al surface transfer electrons to CO molecules, while the doped Fe atom surface absorbs electrons. The result is able to be verified by partial density of states (PDOS) analysis of the models, as shown in Figure 7.

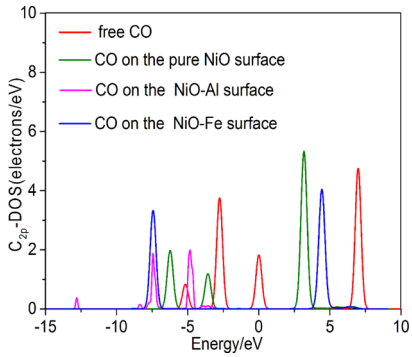

Figure 7. PDOS for the C atom of CO before and after adsorption on the OC surface.

The adsorption of the CO molecule on the Ni atom is due to the hybridization between the 3d orbital of the Ni atom and 5σ, 2π* orbital of the CO molecule. The molecular orbital of CO moves to the low-grade energy level by the interaction. This phenomenon shows that the adsorption of CO on the surface is stable. The PDOS of the adsorbed CO shows a certain orbital hybridization. It can be seen from the figure that the NiO surface doped with the Al atom is more conducive to the transfer of electrons near the Fermi level, which will be conducive to chemical reactions, with better activity. Qin et al. reported that the Al−O structure can be used as a good electron donor, making the active components difficult to agglomerate and promoting the progress of the reaction.[41]

Generally, since the 5σ orbitals and 2π* orbitals of the CO molecule is mainly derived from the C atom, the C atom is more inclined to bond with surface metals.[41] As shown in Figure 7, for the DOS of the unadsorbed CO molecule, there are mainly four peaks of about 7.0, 0, −2.7, and 5.2 eV, corresponding to 2π*, 5σ, 1π, and 4σ orbitals, respectively. Among them, 5σ, 1π, and 4σ orbitals are the bonding orbitals, and the 2π* orbital is the anti-bonding orbital. When the interaction between the CO molecule and Ni-based OC surface occurs, the DOS of the CO molecule is shifted to the left due to the splitting of the outer orbital of the C atom with partially filled electrons. In addition, due to the interaction between the CO molecule and the surface of the OC, the 5σ and 2π* orbitals of the C atom tend to diffuse.[36] Comparison of the CO DOS before and after adsorption indicates a strong interaction between the CO molecule and the surface of the Ni-based OC, which is consistent with the results of adsorption energy; the greater the adsorption energy, the more serious the deviation. This conclusion is consistent with previous reports on CO adsorption.[42]

3.3. Oxidation of CO on the Surface of the Model.

After the CO molecule is stably adsorbed on the surface of OC, it is oxidized to form CO_2 under the action of OC. The oxidized structure is shown in Figure 8. It is related to two elementary reaction steps: CO adsorption and CO_2 desorption.

$$CO + * \rightarrow CO^* \quad (7)$$

$$CO^* + O \rightarrow CO_2 \quad (8)$$

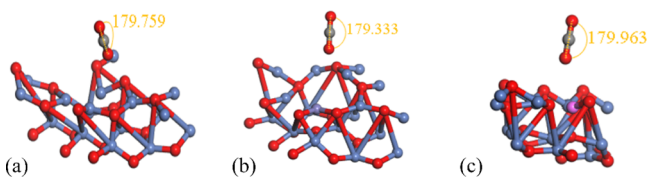

Figure 8. CO_2 model generated by oxidation on the (a) pure NiO(100), (b) NiO(100)−Fe, and (c) NiO(100)−Al surfaces.

Figure 9 presents three reaction mechanisms on the pure surface and doping surface based on the NiO−Fe and NiO−Al reactant. The energy barrier of CO oxidation reaction on the NiO(100) surface is shown in the figure, passing TS1 (TS of CO oxidation reaction on the pure surface). The oxidation energy barrier of the pure surface is located in the middle, and the value is 16.91 eV; thus, doping other atoms has different effects on the oxidation of CO. It can be seen from Figure 8 that the bond angle of O−C−O on the Al-doped surface is about 179.963°, which is the closest to a stable CO_2 molecule. Moreover, the oxidation reaction energy barrier on the NiO−Al surface is the lowest among these three paths, which is 14.33 eV, so doping with Al atoms can promote the oxidation of the CO molecule. The overall reaction is exothermic, indicating that the product is more stable. The produced CO_2 diffuses into the gas phase immediately to promote CO conversion into CO_2. On the contrary, the energy barrier of CO oxidation reaction on the surface of doped Fe atoms is higher than that

https://doi.org/10.1021/acsomega.1c06182
ACS Omega 2022, 7, 4381−4388

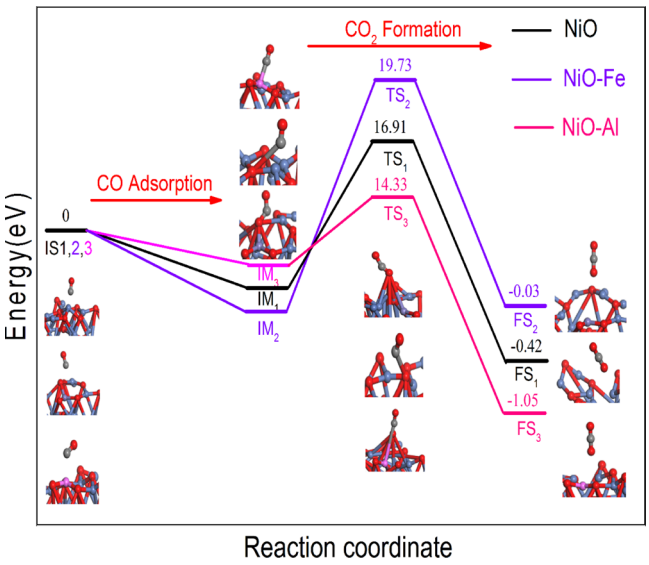

Figure 9. Calculated potential energy profiles for CO oxidation on the OC surface.

on the pure NiO surface, reaching 19.73 eV, which inhibits the reaction. This is consistent with the results of DOS analysis. It can be seen from Figure 7 that the 2p orbital of the C atom is farther away from the Fermi level on the Fe-doped surface than on the pure surface, and the adsorption of CO on the NiO−Fe surface is an electron loss process, which is not conducive to the reaction of the CO molecule. Ma et al. also confirmed that due to the Fe segregation, NiO−Fe OCs need to add other components to improve reducibility, oxygen mobility, and recyclability.[31] This indicates that it is possible to inhibit the CO oxidation reaction process by certain specific structures.

Moreover, in addition to CO_2, carbonate structures will also be formed on the Al-doped surface, as shown in Figure 10. The CO molecule combines with the two oxygen atoms adjacent to the Al atom to form upright carbonate species. This carbonate formation process is significantly exothermic by 0.42 eV, and the reaction energy barrier is 0.12 eV. It should be reinforced that the surface structure plays an important role in the formation and property of the carbonate species.[41] Qin also reported that the chemical bonds are formed after the CO molecule adsorbed on the surface of OC, which is the crucial step for carbon monoxide oxidation, and then, the carbonate species desorb from the OC surface to form the CO_2 molecule.[43]

3.4. Carbon Deposition. In addition to the oxidation reaction, CO molecules will also decompose to form carbon deposits under the catalysis of OC. Carbon deposition has a great influence on the performance of the OC, which will block the channel of the OC and affect the transmission of lattice oxygen. Therefore, research on the carbon deposition effect is critical to improving the performance of OC. The structure after CO decomposition is shown in Figure 11. It is worth mentioning that with CO decomposed on the Al-doped surface, the C atom is in a free state, which is not adsorbed on the OC surface. It means that C atom and O atom on the Al-doped surface are more likely to combine to regenerate the CO molecule. Figure 12 shows the carbon deposition process of CO on different surfaces.

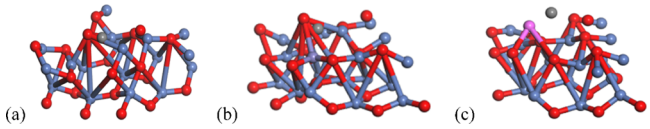

Figure 11. Formation of carbon deposition on the (a) pure NiO(100), (b) NiO(100)−Fe, and (c) NiO(100)−Al surfaces.

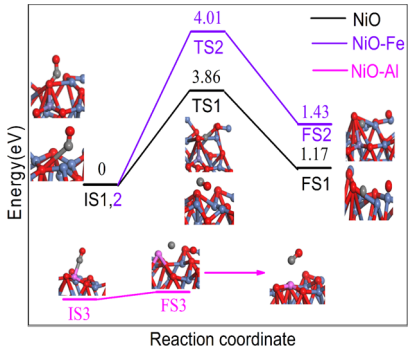

Figure 12. Calculated potential energy profiles for carbon deposition on the OC surface.

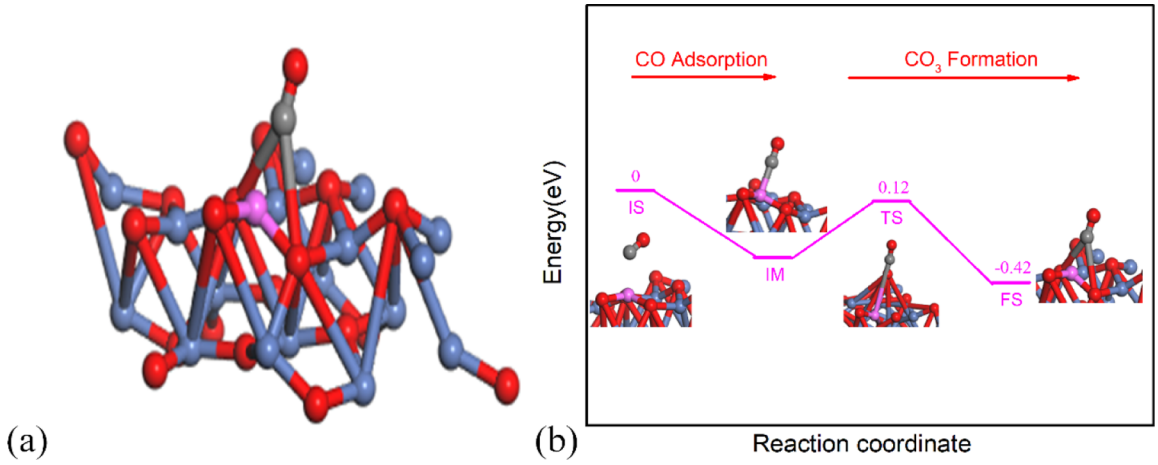

Figure 10. Formation of carbonate species on the NiO−Al surface; (a) model of carbonate; (b) reaction pathway.

https://doi.org/10.1021/acsomega.1c06182
ACS Omega 2022, 7, 4381−4388

The decomposition reaction of CO on the pure NiO surface is an endothermic reaction with a value of 1.17 eV, and the reaction energy barrier is 3.86 eV. On the surface of doped Fe, the energy barrier of CO decomposition reaction is increased by 0.15 eV, and it is also an endothermic process. More heat is absorbed, indicating that Fe atoms have an unfavorable effect on the decomposition reaction of CO, which will alleviate the carbon deposition problem in the deep chemical looping process to a certain extent. The possible reason is that the Fe atoms doped on the surface will create steric hindrance to the O atom decomposed by CO, thereby promoting the recombination of C and O atoms from CO, which will also inhibit the decomposition of CO.[44] The same is true for doped Al surfaces. The resulting steric hindrance makes C atoms free, which can better inhibit carbon deposition. By controlling the content of nickel, the type and content of the carrier, and the synthesis method, suitable surface active sites could be obtained. Because Al species could not only adjust the electronic donor intensity of Ni-based OCs but also increase the basic sites, Al doping can inhibit the formation of carbon deposition.[45] The OCs modified by the inert support carrier could change the interaction between Ni and lattice oxygen, thereby affecting the reactivity of NiO.

3.5. Oxygen Diffusion. After the CO molecule oxidized, oxygen vacancy is formed on the surface of OC. In the subsequent reaction, the lattice oxygen in the bulk phase of the OC will diffuse to the surface and continue to participate in the reaction. Therefore, the diffusion process of lattice oxygen will significantly affect the OC reactivity performance. The oxygen diffusion reaction processes and energy profiles are shown in Figure 13. The elementary reaction is as follows (O_L as the inner lattice oxygen and O_S as the surface oxygen)

$$O_L(NiO) \rightarrow O_S(NiO) \tag{9}$$

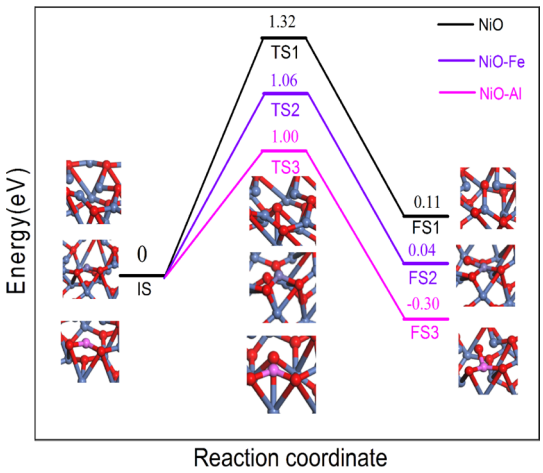

Figure 13. Oxygen diffusion reaction processes and energy profiles in OC.

It can be seen from Figure 13 that the oxygen transfer energy barrier is reduced after doping with other atoms, indicating that the lattice oxygen transfer is easier after doping with Fe and Al atoms. It is worth mentioning that the doping of Fe atoms is not conducive to the oxidation of CO from the above results. However, as the reaction progresses, the subsequent oxygen transfer is promoted, the reaction energy barrier drops to 1.06 eV, and the total endothermic heat of the reaction is also reduced, which may be more conducive to the subsequent oxidation reaction. With the doping of Al atoms promoting oxygen transfer more obviously, the reaction energy barrier is reduced to 1.00 eV, the total reaction also becomes an exothermic reaction, and the process of transferring oxygen atoms releases 0.30 eV of heat. The transfer of lattice oxygen relates to the bond length and bond energy of the Ni−O bond. Hossain et al. verified that the inert support could increase the reactivity of OCs mainly by enhancing the diffusivity of oxygen anions.[27] Nieva et al. verified that Al_2O_3 as a support can make the Ni-based OC release lattice oxygen more effective, thereby preventing sintering and inhibiting formation of carbon-containing deposits.[46] Therefore, doping with other atoms facilitates the transfer of bulk lattice oxygen after the formation of oxygen vacancies and promotes the subsequent chemical looping process.

3.6. Comparison between Each Processes within NiO and Modification Surface. Base on the DFT calculations, there are three reaction processes on the Ni-base surface. As shown in Figure 14, the energy barriers of CO_2 formation (step 1), carbon deposition (step 2), and oxygen diffusion (step 3) processes on pure NiO and two doping NiO surface are compared to analyze the effect of modification of metal (Fe, Al) doping to reaction activity of the Ni-based OC. It is worth noting that since no carbon deposits form on the Al-doped surface, there is no NiO−Al pattern in the S2 process.

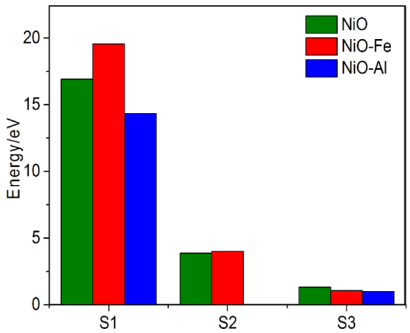

Figure 14. Energy barriers of CO_2 formation (S1), carbon deposition (S2), and oxygen diffusion (S3) processes.

The comparison shows that the energy barrier of CO oxidation to CO_2 is much higher than the energy barrier of CO decomposition to produce carbon deposition and even higher than that for carbonate formation. This indicates that the surface of the Ni-based OC exhibits weak oxidizing properties. However, the diffusion of internal lattice oxygen only needs to surmount the low energy barrier, which beneficially affects the reaction performance of the nickel-based OC. Therefore, in order to increase the CO reaction activity of nickel-based OCs, it is necessary to find modified components that could reduce the energy barrier of CO_2 formation.

The key controlling step of the syngas generation reaction process is the CO oxidation. Therefore, the suitable ratio of H_2/CO largely depends on the oxidizing ability of the OC. The research of Yuan et al. proved that the formation of H_2 on the surface of NiO is easier than the oxidation of CO, and NiO presents higher selectivities with the enhancement ratio of H_2/CO of the syngas.[36] The reactivity between the components in general syngas and the NiO OC with high performance is as follows: H_2 > CO > CH_4.[47] Therefore, it can be roughly inferred that the higher energy barrier of the CO oxidation

https://doi.org/10.1021/acsomega.1c06182
ACS Omega 2022, 7, 4381−4388

process is more conducive to hydrogen production. Moreover, a previous study indicated that the inert support was able to enhance the reaction activity of OC mainly through the enhancement of lattice oxygen diffusivity.[48] As a result, the selectivity of the inert support has important influence for the Ni-based OC. Our calculation results could provide an important basis for understanding the criticality of surface reactions and be used as an important basis for rationally improving the performance of nickel-based OCs.

4. CONCLUSIONS

This paper used periodic DFT to study the adsorption, oxidation, and decomposition reaction mechanism of the CO molecule on NiO(100) and its doping surfaces. The results show that in the chemical looping process, the electron density of the adsorption site and the redistribution of the adsorptive CO electrons are adjusted to induce related reactions. Al doping modification helps to increase the reactivity of NiO(100) surface and reduce the energy barrier of CO oxidation. CO molecules on the Al-doped surface are easily oxidized by surface oxygen to form CO_2 molecules, which is due to its low energy barrier. For the dissociation of the CO molecule and the process of carbon deposition, the Fe-doped surface raises the energy barrier of the carbon deposition reaction, and no carbon deposition is formed on the Al-doped surface. The diffusion energy barrier of oxygen on the modified surface is quite low, indicating that doping with other atoms is beneficial to the diffusion of lattice oxygen in NiO. Therefore, research on the metal composition, doping ratio, and method of the modified nickel-based OC will provide a certain theoretical basis for the development and optimization of the OC in the CLC process.

■ AUTHOR INFORMATION

Corresponding Authors

Wenguo Xiang − *Key Laboratory of Energy Thermal Conversion and Control of Ministry of Education, School of Energy and Environment, Southeast University, Nanjing 210096, China;* orcid.org/0000-0001-9989-0936; Email: wgxiang@seu.edu.cn

Shiyi Chen − *Key Laboratory of Energy Thermal Conversion and Control of Ministry of Education, School of Energy and Environment, Southeast University, Nanjing 210096, China;* orcid.org/0000-0002-2155-9167; Email: sychen@seu.edu.cn

Author

Shubo Chen − *Key Laboratory of Energy Thermal Conversion and Control of Ministry of Education, School of Energy and Environment, Southeast University, Nanjing 210096, China*

Complete contact information is available at: https://pubs.acs.org/10.1021/acsomega.1c06182

Notes

The authors declare no competing financial interest.

■ ACKNOWLEDGMENTS

This work was supported by National Key Research and Development Program of China [grant number 2018YFB0605403] and Design Study of Hydrogen-rich Fuel Production, HAT Characteristics and Specific Test Application in HiGT [grant number BM2019001].

■ REFERENCES

(1) Zheng, Z.; Luo, L.; Feng, A.; Iqbal, T.; Li, Z.; Qin, W.; Dong, C.; Zhang, S.; Xiao, X. CaO-Assisted Alkaline Liquid Waste Drives Corn Stalk Chemical Looping Gasification for Hydrogen Production. *ACS Omega* **2020**, *5*, 24403−24411.

(2) Qin, W.; Luo, L.; Chen, S.; Iqbal, T.; Xiao, X.; Dong, C. Efficient strategy of utilizing alkaline liquid waste boosting biomass chemical looping gasification to produce hydrogen. *Fuel Process. Technol.* **2021**, *217*, 106818.

(3) Qin, W.; Chen, S.; Ma, B.; Wang, J.; Li, J.; Liang, R.; Xu, Z.; Liu, L.; Dong, C.; Zhang, H. Methanol solution promoting cotton fiber chemical looping gasification for high H_2/CO ratio syngas. *Int. J. Hydrogen Energy* **2019**, *44*, 7149−7157.

(4) Kevat, M. D.; Banerjee, T. Process Simulation and Energy Analysis of Chemical Looping Combustion and Chemical Looping with Oxygen Uncoupling for Sawdust Biomass. *Energy Technol.* **2018**, *6*, 1237−1247.

(5) Zeng, L.; Cheng, Z.; Fan, J. A.; Fan, L.-S.; Gong, J. Metal oxide redox chemistry for chemical looping processes. *Nat. Rev. Chem.* **2018**, *2*, 349−364.

(6) Wang, L.; Li, Q.; Qin, W.; Zheng, Z. M.; Xiao, X. B.; Dong, C. Q. Activity of Fe_2O_3 and its effect on co oxidation in the chemical looping combustion: an theoretical account, Advanced Materials Research. *Trans. Tech. Publ.* **2013**, *726−731*, 2040−2044.

(7) Cai, X.; Wang, X.; Guo, X.; Zheng, C.-G. Mechanism study of reaction between CO and NiO (001) surface during chemical-looping combustion: role of oxygen. *Chem. Eng. J.* **2014**, *244*, 464−472.

(8) Mishra, A.; Li, F. Chemical Looping at the Nanoscale-Challenges and Opportunities. *Curr. Opin. Chem. Eng.* **2018**, *20*, 143−150.

(9) Bayham, S. C.; Tong, A.; Kathe, M.; Fan, L.-S. Chemical Looping Technology for Energy and Chemical Production. *Wiley Interdiscip. Rev.: Energy Environ.* **2016**, *5*, 216−241.

(10) Hu, J.; Chen, S.; Xiang, W. Sintering and agglomeration of Fe_2O_3-$MgAl_2O_4$ oxygen carriers with different Fe_2O_3 loadings in chemical looping processes. *Fuel* **2020**, *265*, 116983.

(11) Zeng, L.; Cheng, Z.; Fan, J. A.; Fan, L.-S.; Gong, J. Metal Oxide Redox Chemistry for Chemical Looping Processes. *Nat. Rev. Chem.* **2018**, *2*, 349−364.

(12) Yuan, Y.; You, H.; Ricardez-Sandoval, L. Recent advances on first-principles modeling for the design of materials in CO_2 capture technologies. *Chin. J. Chem. Eng.* **2019**, *27*, 1554−1565.

(13) Cho, P.; Mattisson, T.; Lyngfelt, A. Comparison of iron-, nickel-, copper-and manganese-based oxygen carriers for chemical-looping combustion. *Fuel* **2004**, *83*, 1215−1225.

(14) Mattisson, T.; Lyngfelt, A.; Cho, P. The use of iron oxide as an oxygen carrier in chemical-looping combustion of methane with inherent separation of CO_2. *Fuel* **2001**, *80*, 1953−1962.

(15) Wang, M.; Liu, J.; Hu, J.; Liu, F. O_2-CO_2 mixed gas production using a Zr-doped cubased oxygen carrier. *Ind. Eng. Chem. Res.* **2015**, *54*, 9805−9812.

(16) Park, J. H.; Hwang, R. H.; Rasheed, H. u.; Baek, J. I.; Ryu, H. J.; Yi, K. B. Kinetics of the reduction and oxidation of Mg added NiO/Al_2O_3 for chemical looping combustion. *Chem. Eng. Res. Des.* **2019**, *141*, 481−491.

(17) Lin, S.; Gu, Z.; Zhu, X.; Wei, Y.; Long, Y.; Yang, K.; He, F.; Wang, H.; Li, K. Synergy of red mud oxygen carrier with MgO and NiO for enhanced chemical-looping combustion. *Energy* **2020**, *197*, 117202.

(18) Tijani, M. M.; Ehsan, M.; Nader, M. Process simulation and thermodynamic analysis of a chemical looping combustion system using methane as fuel and NiO as the oxygen carrier in a moving-bed reactor. *Chem. Eng. Process.* **2019**, *144*, 107636.

(19) Long, Y.; Gu, Z.; Lin, S.; Yang, K.; Zhu, X.; Wei, Y.; Wang, H.; Li, K. NiO and CuO coated monolithic oxygen carriers for chemical looping combustion of methane. *J. Energy Inst.* **2021**, *94*, 199−209.

(20) Blas, L.; Sophie, D.; Laure, M.; Patrick, D.; Arnold, L.; David, C.; Stéphane, B. Influence of the regeneration conditions on the performances and the microstructure modifications of NiO/$NiAl_2O_4$ for chemical looping combustion. *Fuel* **2015**, *153*, 284−293.

(21) Sedghkerdar, M. H.; Davood, K.; Nader, M. Reduction and oxidation kinetics of solid fuel chemical looping combustion over a core-shell structured nickel-based oxygen carrier: Application of a developed grain size distribution model. *Fuel* **2020**, *274*, 117838.
(22) Zhang, H.; Hong, H.; Jiang, Q.; Deng, Y. n.; Jin, H.; Kang, Q. Development of a chemical-looping combustion reactor having porous honeycomb chamber and experimental validation by using $NiO/NiAl_2O_4$. *Appl. Energy* **2018**, *211*, 259−268.
(23) Moheddin, M.-E.; Mansour, M.-T.; Nader, M. Characterization, kinetics and stability studies of NiO and CuO supported by Al_2O_3, ZrO_2, CeO_2 and their combinations in chemical looping combustion. *Catal. Today* **2021**, DOI: 10.1016/j.cattod.2021.09.035.
(24) Sun, D.; Gu, X.-K.; Ouyang, R.; Su, H.-Y.; Fu, Q.; Bao, X.; Li, W.-X. Theoretical study of the role of a metal−cation Ensemble at the Oxide−Metal Boundary on CO oxidation. *J. Phys. Chem. C* **2012**, *116*, 7491−7498.
(25) Wang, X.; Chen, Z.; Hu, M.; Tian, Y.; Jin, X.; Ma, S.; Xu, T.; Hu, Z.; Liu, S.; Guo, D.; Xiao, B. Chemical looping combustion of biomass using metal ferrites as oxygen carriers. *Chem. Eng. J.* **2017**, *312*, 252−262.
(26) Deng, G.; Li, K.; Gu, Z.; Zhu, X.; Wei, Y.; Cheng, X.; Wang, H. Synergy effects of combined red muds as oxygen carriers for chemical looping combustion of methane. *Chem. Eng. J.* **2018**, *341*, 588−600.
(27) Hossain, M. M.; de Lasa, H. I. Reduction and oxidation kinetics of Co-Ni/Al_2O_3 oxygen carrier involved in a chemical looping combustion cycles. *Chem. Eng. Sci.* **2010**, *65*, 98−106.
(28) Qin, L.; Cheng, Z.; Guo, M.; Xu, M.; Fan, J.-A.; Fan, L.-S. Impact of 1% lanthanum dopant on carbonaceous fuel redox reactions with an iron-based oxygen carrier in chemical looping processes. *ACS Energy Lett.* **2017**, *2*, 70−74.
(29) Qin, L.; Guo, M.; Cheng, Z.; Xu, M.; Liu, Y.; Xu, D.; Fan, J. A.; Fan, L.-S. Improved cyclic redox reactivity of lanthanum modified iron-based oxygen carriers in carbon monoxide chemical looping combustion. *J. Mater. Chem. A* **2017**, *5*, 20153−20160.
(30) Kuo, Y.-L.; Hsu, W.-M.; Chiu, P.-C.; Tseng, Y.-H.; Ku, Y. Assessment of redox behavior of nickel ferrite as oxygen carriers for chemical looping process. *Ceram. Int.* **2013**, *39*, 5459−5465.
(31) Ma, Z.; Zeng, D.; Zhang, S.; Xiao, R. Effect of Supports on the Redox Performance of $NiFe_2O_4$ in a Chemical Looping Process. *Energy Technol.* **2019**, *7*, 1900374.
(32) Qin, W.; Luo, L.; Feng, A.; Xiao, X.; Dong, C. Ammonia deep chemical looping combustion on perfect and reduced Fe_2O_3: A theoretical account. *Int. J. Energy Res.* **2021**, *45*, 10562−10571.
(33) Luo, L.; Zheng, X.; Wang, J.; Qin, W.; Xiao, X.; Zheng, Z. Catalyzed Ethanol Chemical Looping Gasification Mechanism on the Perfect and Reduced Fe_2O_3 Surfaces. *Energies* **2021**, *14*, 1663.
(34) Liang, Z.-Y.; Qin, W.; Shi, S. Modification of Co-doping on reaction properties of Fe_2O_3(104) oxygen carrier during chemical looping combustion. *Adv. Eng. Sci.* **2019**, *51*, 28−35.
(35) Yuan, Y.; Dong, X.; Ricardez-Sandoval, L. A multi-scale simulation of syngas combustion reactions by Ni-based oxygen carriers for chemical looping combustion. *Appl. Surf. Sci.* **2020**, *531*, 147277.
(36) Yuan, Y.; Dong, X.; Ricardez-Sandoval, L. Insights into Syngas Combustion on a Defective NiO Surface for Chemical Looping Combustion: Oxygen Migration and Vacancy Effects. *J. Phys. Chem. C* **2020**, *124*, 28359−28370.
(37) Yuan, Y.; Dong, X.; Ricardez-Sandoval, L. A density functional theory analysis on syngas adsorption on NiO (100) surface. *Appl. Surf. Sci.* **2019**, *498*, 143782.
(38) White, J. A.; Bird, D. M. Implementation of gradient-corrected exchange-correlation potentials in car-Parrinello total-energy calculations. *Phys. Rev. B: Condens. Matter Mater. Phys.* **1994**, *50*, 4954−4957.
(39) Perdew, J. P.; Chevary, J. A.; Vosko, S. H.; Jackson, K. A.; Pederson, M. R.; Singh, D. J.; Fiolhais, C. Atoms, molecules, solids, and surfaces: applications of the generalized gradient approximation for exchange and correlation. *Phys. Rev. B: Condens. Matter Mater. Phys.* **1992**, *46*, 6671−6687.
(40) Zhou, L.; Xiu, F.; Qiu, M.; Xia, S.; Yu, L. The adsorption and dissociation of water molecule on goethite (010) surface: a DFT approach. *Appl. Surf. Sci.* **2017**, *392*, 760−767.
(41) Qin, W.; Wang, Y.; Dong, C.; Zhang, J.; Chen, Q.; Yang, Y. The synergetic effect of metal oxide support on Fe_2O_3 for chemical looping combustion: A theoretical study. *Appl. Surf. Sci.* **2013**, *282*, 718−723.
(42) Shi, X.; Bernasek, S. L.; Selloni, A. Formation, electronic structure, and defects of Ni substituted spinel cobalt oxide: a DFT+U study. *J. Phys. Chem. C* **2016**, *120*, 14892−14898.
(43) Tan, Q.; Qin, W.; Chen, Q.; Dong, C.; Li, W.; Yang, Y. Synergetic effect of ZrO_2 on the oxidation−reduction reaction of Fe_2O_3 during chemical looping combustion. *Appl. Surf. Sci.* **2012**, *258*, 10022−10027.
(44) Li, J.-H.; Lin, C.-F.; Lin, C.-F.; Qin, W.; Xiao, X.-B.; Wei, L. Synergetic Effect of Mercury Adsorption on the Catalytic Decomposition of CO over Perfect and Reduced Fe_2O_3[001] Surface. *Acta Phys. Chim. Sin.* **2016**, *32*, 2717−2723.
(45) Wang, Y.; Yao, L.; Wang, S.; Mao, D.; Hu, C. Low-temperature catalytic CO2 dry reforming of methane on Ni-based catalysts: A review. *Fuel Process. Technol.* **2018**, *169*, 199−206.
(46) Nieva, M. A.; María, M.; Antonio, M.; Teresita, F.-G.; Alberto, J.-M. Steam-methane reforming at low temperature on nickel-based catalysts. *Chem. Eng. J.* **2014**, *235*, 158−166.
(47) Ahmed, I.; de Lasa, H. 110th Anniversary: Kinetic Model for Syngas Chemical Looping Combustion Using a Nickel-Based Highly Performing Fluidizable Oxygen Carrier. *Ind. Eng. Chem. Res.* **2019**, *58*, 2801−2811.
(48) Li, F.; Luo, S.; Sun, Z.; Bao, X.; Fan, L.-S. Role of metal oxide support in redox reactions of iron oxide for chemical looping applications: experiments and density functional theory calculations. *Energy Environ. Sci.* **2011**, *4*, 3661−3667.

https://doi.org/10.1021/acsomega.1c06182
ACS Omega 2022, 7, 4381−4388